Stretchable Field-Effect-Transistor Array of Suspended SnO$_2$ Nanowires

Gunchul Shin, Chang Hoon Yoon, Min Young Bae, Yoon Chul Kim, Sahng Ki Hong, John A. Rogers,* and Jeong Sook Ha*

Recently, various future devices including microelectronics and bioimplantable devices have been designed as curvilinear layouts on curved or stretchable surfaces of skin or organs.[1–4] Silicon and polymer-based organics have been used primarily for commercial flat/rigid electronics and for curvilinear flexible/stretchable electronics.[2,5] However, 1D materials such as nanowires (NWs) are expected to be advantageous in future, stretchable electronics, exhibiting increased performance and better integration due to their superior electronic properties and structurally high aspect ratios.[6] In this work, we report the fabrication of high-performance, stretchable, electronic devices with suspended NWs, which demonstrate great potential for applications in wearable or bioimplantable devices.

Diluted poly-amic acid solution was spin-coated onto a common SiO$_2$/Si substrate and annealed following the previously reported recipe[1] to make an approximately 300 nm-thick polyimide (PI) layer, as shown in **Scheme 1**. Because of the very low adhesion between SiO$_2$ ($\gamma \approx 0.2$ J m^{-2})[7] and PI ($\gamma \approx 37.4$ mJ m^{-2}),[8] the first polyimide layer was coated underneath the device for easy detachment. After deposition and patterning of the gate electrode, the second polyimide layer also was spin-coated on the bottom-gate as a temporary gate insulator. Thus, the gate metal electrodes were encapsulated by two PI layers, which place the metal interconnects in a nearly neutral mechanical plane to minimize expansive/compressive strain.[1] SnO$_2$ NWs were synthesized by chemical vapor deposition (CVD) and transferred onto a photoresist prepatterned substrate via a sliding transfer technique.[9] Au was evaporated to fabricate the source and drain electrodes, which define the channel length and width of 5 and 160 μm, respectively. To improve the deformability and to reduce strain in the devices, the metal interconnects were formed in curves, which is expected to accommodate applied strain more effectively.[1,2] Therefore, the curved interconnects were stretched, prohibiting the deformation of the whole device while the device extends with applied strain.

When the PI layer was exposed to oxygen plasma, suspended NW structures were formed by etching the PI layer underneath the NW channels. Although the lateral etching rate was expected to be much smaller than the vertical etching rate, it was sufficient to completely remove the PI layer directly underneath the NWs within 7 min (O$_2$ gas flow rate = 20 standard cubic centimeters per minute (sccm), process pressure = 50 mTorr (where 1 Torr ≈ 133 Pa), and radio frequency (RF) power = 150 W). Finally, the whole device was detached from the silica surface via the tape transfer method, facilitated by the poor adhesion between PI and silica: devices detached with tape barely contact the stretchable polydimethylsiloxane (PDMS) polymer, resulting in easy transfer of the devices.

Figure 1a shows the optical microscope image and the scanning electron microscopy (SEM) image taken from the fabricated device; the NWs are well aligned along the channel direction, and the curved interconnects are confirmed. The average density (D) of NWs in the channel was estimated to be 2 NWs per micrometer. Each SnO$_2$ NW field-effect transistor (FET) consisted of an active device unit and a neighboring electrode unit for electrical probing. All the interconnections were designed in a helical shape. When the whole device was compressed or extended, the curved interconnection relaxed the applied strain by stretching itself, instead of stretching the active unit. Because of the weak adhesion between the substrate and PI layer, whole devices and surrounding dummy areas were easily detached from the conventional SiO$_2$/Si substrate by the tape transfer method. After attaching the commercial tape (plastic tape, 3M) on the edge of the substrate—not on the device (Figure 1b)—the tape and the whole device layer were completely detached from the substrate. Figure 1b shows the detached device with tape and the subsequent clean substrate. Finally, the tape was attached to the PDMS substrate, and the residual PI pattern was removed by oxygen plasma etching. A suspended NW structure was confirmed by obtaining slightly tilted SEM images of the devices prior to and after the O$_2$ etching. As shown in the top image of Figure 1c, SnO$_2$ NWs originally sat on the PI gate dielectric layer. After the O$_2$ etching, the PI layer no longer existed under the SnO$_2$ NWs, as shown in the bottom image of Figure 1c. As shown, most NWs floated

G. Shin, C. H. Yoon, M. Y. Bae, Y. C. Kim, S. K. Hong, Prof. J. S. Ha
Department of Chemical and Biological Engineering
Korea University
Seoul 136-701, Korea
E-mail: jeongsha@korea.ac.kr

Prof. J. A. Rogers
Department of Materials Science and Engineering
Frederick Seitz Materials Research Laboratory
and Beckman Institute for Advanced Science and Technology
University of Illinois at Urbana-Champaign
Urbana, IL 61801, USA
E-mail: jrogers@uiuc.edu
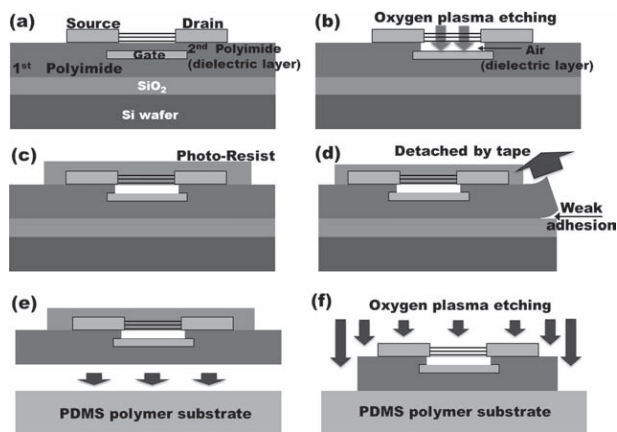
Scheme 1. Schematics of stretchable nanowire device fabrication. a) Bottom-gate SnO_2 NW FET. b) O_2 plasma etching for the suspended NW structure. c) Photoresist coating on the device area for additional polymer etching. d) Detaching of the whole device from the substrate by plastic tape. e) Contacting the detached device onto the PDMS with van der Waals forces. f) O_2 plasma etching of the coated photoresist.

above the bare gate electrode, while both ends were held tight by the source and drain electrodes. But these NWs were slightly deflexed possibly due to gravity after the removal of the supporting PI layer.

The gate-dependent behavior of the device became totally different after O_2 plasma etching. FETs with a 300 nm-thick PI dielectric layer showed a weak dependence on the gate bias between –5 and +5 V. Only when the sweep range of the gate bias was increased up to ±40 V was a distinguishable gate-bias-dependent transfer curve obtained with a current on/off ratio of 10^4 (Supporting Information (SI), Figure S5). Conversely, after O_2 plasma etching, the FETs exhibited a strong gate-dependence of the transfer property in the small

gate bias between –5 and +5 V, as shown in Figure 1d. In addition, the on-current (I_{DS}) at V_{GS} = 5 V (voltage between source and gate) increased up to 10^{-5} A, and the current on/off ratio was greater than 10^5 at ±5 V. In summary, suspended NW devices produced ultra-high performance at a small gate bias with a dramatically reduced hysteresis due to the removal of surface-trapped charges in PI.

Detached devices were transferred onto PDMS, a representative soft, flexible, and stretchable polymer. **Figure 2**a shows images of transferred NW FETs. Arrays (9×9) of SnO_2 NW FETs were perfectly transferred without any crack in interconnections or actual devices. When the devices on PDMS were twisted, curved interconnections stretched to accommodate the strain applied to the whole area (Figure 2b), keeping the devices in a well-attached state. Representative electrical properties of NW FETs are shown in Figure 2c,d. FETs showed a strong gate-dependent behavior, which is typical of an n-type semiconductor. In the transfer curve of I_{DS}/V_{DS} (where V_{DS} is the voltage between source and drain), a noticeable variation in the current is observed under a small gate-voltage sweep of 0–3 V. Current on/off ratio at ±3 V and on-current at +3 V were ≈10^6 and 0.1 mA, respectively. Here, a negligible leakage current (I_{GS}) through the gate dielectric was a few nanoamperes. Field-effect mobility of our suspended NW FETs was estimated to be ≈65–450 cm^2 V^{-1} s^{-1}, when using a cylinder-on-plane model[10] with the worst estimated values of variables (dielectric constant, thickness of dielectric layer). Under such circumstances, mobility values are better than that of previously reported SnO_2 NW devices.[11]

Some of the devices (<10%) showed different gate-dependent properties than those represented in the above results. In the channel, there were some short nanowires, which might not have completely bridged the source and drain electrodes. Therefore, those nanowires can be deflexed much more than the long NWs, of which both ends were held tightly by the source and drain electrodes (**Figure 3**a), and they can touch the bare bottom gate electrode due to gravity (Figure 3b). In this case, a huge current was expected to flow between the gate and sunken nanowires, resulting in a very poor on/off current ratio (<10), as shown in Figure 3d. Using an optimized channel length (5 µm in our work; length of NWs tens of micrometers) under dry conditions after fabricating the suspended NW structure, most of the devices (>90%) showed reasonable performance (Figure 3c) without an extraordinarily large leakage current driven by sunken NWs. To reduce the population of such sunken nanowires, the fabrication process can be modified for shorter channel lengths, longer nanowires, and thicker dielectric layers. The use of supercritical drying techniques can also be explored, to minimize the capillary forces that are responsible for the sunken geometries. Since there was a clear difference in transfer curves between
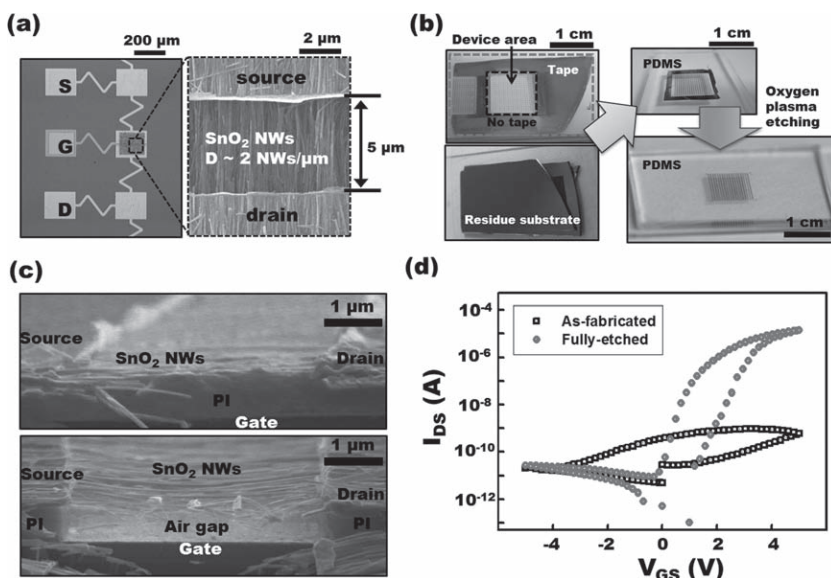
Figure 1. a) Optical microscope and SEM images taken from the fabricated devices and aligned NWs in the channel, respectively. b) Transfer of the FET arrays onto flexible PDMS using plastic tape. c) Tilted cross-sectional SEM images of the SnO_2 NW channel prior to (top) and after (bottom) O_2 reactive ion etching, respectively. d) Transfer curves of SnO_2 NW FET prior to (squares) and after (circles) O_2 reactive ion etching.
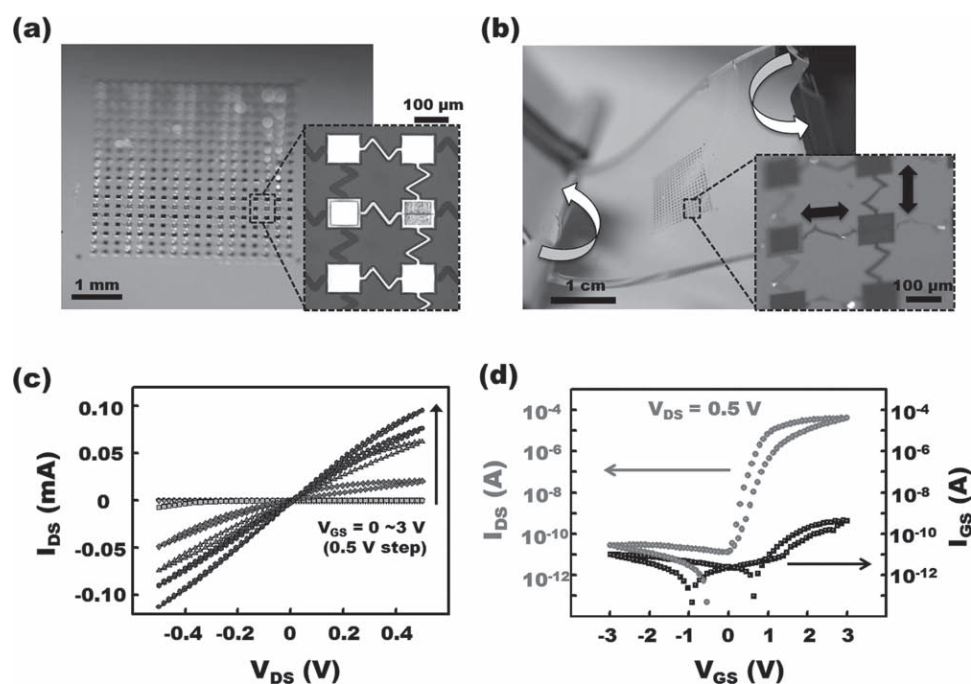
Figure 2. Optical microscope and SEM images of a) an SnO$_2$ NW FET array on PDMS and b) twisted devices on PDMS. Representative c) I_{DS}–V_{DS} curve with variation of gate bias and d) transfer curve of I_{DS} versus V_{GS} (pale circles) and the gate leakage current I_{GS} versus V_{GS} (dark squares).

suspended NWs and sunken NWs, we concluded that such high on-current values of our suspended devices do not originate from the leakage due to the direct contact of NWs with the gate electrode.

Using a home-made, unidirectional stretching stage, PDMS with our NW FETs was stretched up to a strain of 40%, where the compressed strain was applied up to 16% in the perpendicular direction, as shown in **Figure 4**a. In our mechanical designs, the active device regions, including the channel areas, do not experience significant strain when the entire system is stretched, independent of direction. In particular, the devices act as rigid islands that are isolated from

externally applied strains by the surrounding soft elastomer regions. When strain up to 40% was applied, the transfer curve did not change noticeably (Figure 4b). Statistical distribution of the electrical performance under the applied strain was obtained from 13 different FETs. The threshold voltage (V_{Th}) was distributed between 1.2 and 2.0 V, indicating statistical variation, but there was negligible change in V_{Th} with variation in the strain. The subthreshold swing (S.S.) value did not change with the applied strain. Current on/off ratio and mobility values remained almost the same with variation in the strain. As shown in the statistical distribution, there was no noticeable change under complex distributions of strain that involve components along two axes at the same time (up to 40% along the x-axis and up to 16% along the y-axis), even though there was a random fluctuation among individual devices.

In this paper, we report the fabrication of high performance, stretchable FET arrays with suspended SnO$_2$ NWs. We used two mechanical strategies (neutral mechanical plane and curved interconnection) to obtain the stretchability. For the fabrication of suspended NW FET devices, we removed the underlying polymer layer by oxygen plasma etching. These devices demonstrate excellent performance with high field-effect mobilities of $\approx 10^2$ cm^2 V^{-1} s^{-1}, current on/off ratios of $\approx 10^6$, subthreshold swing values of ≈ 0.5 V dec^{-1}, and a small hysteresis compared to nonsuspended NW devices. Such device performance did not deteriorate

Figure 3. Schematics and transfer curves of the suspended NW device (a,c) and sunken NW device (b,d). Transfer curves of I_{DS} versus V_{GS} are shown with a linear scale (dark squares) and a logarithmic scale (pale circles).
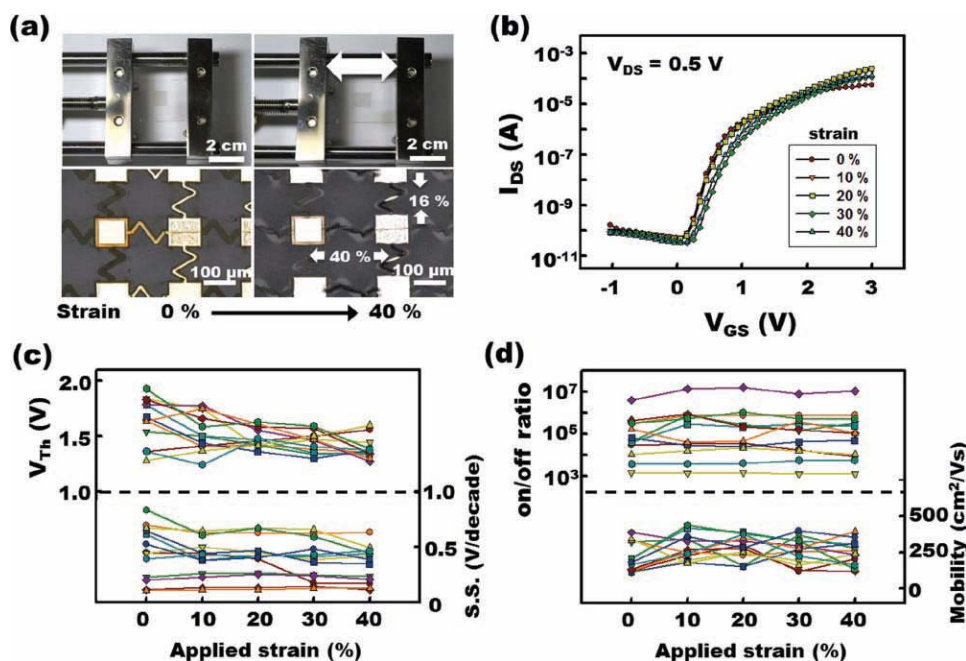
Figure 4. a) Photographs of the unidirectional stretching device with and without stretching (top) and the corresponding optical microscope images of SnO$_2$ NW FET array devices (bottom). Extension of the device by 40% in the *x*-direction causes a 16% contraction in the *y*-direction. b) Transfer curves with variation of applied strain from 0 to 40%. c) Threshold voltage and subthreshold swing change with various strain. d) Current on/off ratio and mobility change with strain. Thirteen different devices (different symbols) were measured for the statistical distribution.

when the devices were stretched up to 40%, demonstrating the robustness of stretchable NW devices.

Experimental Section

Diluted Poly-armic Acid Solution: Poly-armic acid solution (Aldrich) and its base solvent (mixture of 1-methyl-2-pyrrolidinone and aromatic hydrocarbon solvent with a mixing ratio of 80:20, Aldrich) were well mixed with a mixing ratio of 3:1. After mixing, the solution was kept for at least half an hour in a yellow light room. Then it was spin-coated onto a SiO$_2$/Si substrate with a two-step scheme of 500 rpm for 30 s and then 4000 rpm for 1 min. After annealing at 95 °C for 3 min and 150 °C for 10 min to remove the residual solvent, it was heated at 250 °C for 2 h under argon atmosphere for cross-linking to form a polyimide film.

Growth of SnO$_2$ Nanowires: SnO$_2$ nanowires were grown by CVD with a vapor–liquid–solid mechanism in a home-made furnace. CVD growth conditions were as follows: growth temperature of 750 °C, oxygen flow of 0.5 sccm, and 5 nm-thick Au film catalysts.

Sliding Transfer of SnO$_2$ NWs: SnO$_2$ nanowires were transferred from a donor substrate to an acceptor device substrate using a home-made sliding transfer machine. Donor and acceptor substrates (target substrate) were slid in opposite directions with an applied pressure of 1.0 kg cm^{-2} and a speed of 20 mm min^{-1}.

Supporting Information

Supporting Information is available from the Wiley Online Library or from the author.

[1] a) D.-H. Kim, J. A. Rogers, *Adv. Mater.* **2008**, *20*, 4887; b) D.-H. Kim, Z. Liu, Y.-S. Kim, J. Wu, J. Song, H.-S. Kim, Y. Huang, K.-C. Hwang, Y. Zhang, J. A. Rogers, *Small* **2009**, *5*, 2841; c) D.-H. Kim, J.-H. Ahn, W.-M. Choi, H.-S. Kim, T.-H. Kim, J. Song, Y. Y. Huang, L. Zhuangjian, L. Chun, J. A. Rogers, *Science* **2008**, *320*, 507.

[2] a) H. C. Ko, M. P. Stoykovich, J. Song, V. Malyarchuk, W. M. Choi, C.-J. Yu, J. B. Geddes, J. Xiao, S. Wang, Y. Huang, J. A. Rogers, *Nature* **2008**, *454*, 748; b) H. C. Ko, G. Shin, S. Wang, M. P. Stoykovich, J. W. Lee, D.-H. Kim, J. S. Ha, Y. Huang, K.-C. Hwang, J. A. Rogers, *Small* **2009**, *5*, 2703; c) I. Jung, G. Shin, V. Malyarchuk, J. S. Ha, J. A. Rogers, *Appl. Phys. Lett.* **2010**, *96*, 021110; d) G. Shin, I. Jung, V. Malyarchuk, J. Song, S. Wang, H. C. Ko, Y. Huang, J. S. Ha, J. A. Rogers, *Small* **2010**, *6*, 851.

[3] S.-I. Park, Y. Xiong, R.-H. Kim, P. Elvikis, M. Meitl, D.-H. Kim, J. Wu, J. Yoon, C.-J. Yu, Z. Liu, Y. Huang, K.-C. Hwang, P. Ferreira, X. Li, K. Choquette, J. A. Rogers, *Science* **2009**, *325*, 977.

[4] a) D.-H. Kim, Y.-S. Kim, J. Amsden, B. Panilaitis, D. L. Kaplan, F. G. Omenetto, M. R. Zakin, J. A. Rogers, *Appl. Phys. Lett.* **2009**, *95*, 133701; b) J. Viventi, D.-H. Kim, J. D. Moss, Y.-S. Kim, J. A. Blanco, N. Annetta, A. Hicks, J. Xiao, Y. Huang, D. J. Callans, J. A. Rogers, B. Litt, *Sci. Transl. Med.* **2010**, *2*, 24ra22; c) D.-H. Kim, J. Viventi, J. J. Amsden, J. Xiao, L. Vigeland, Y.-S. Kim, J. A. Blanco, B. Panilaitis, E. S. Frechette, D. Contreras, D. L. Kaplan, F. G. Omenetto, Y. Huang, K.-C. Hwang, M. R. Zakin,

B. Litt, J. A. Rogers, *Nat. Mater.* **2010**, *9*, 511; d) R.-H. Kim, D.-H. Kim, J. Xiao, B. H. Kim, S.-I. Park, B. Panilaitis, R. Ghaffari, J. Yao, M. Li, Z. Liu, V. Malyarchuk, D. G. Kim, A.-P. Le, R. G. Nuzzo, D. L. Kaplan, F. G. Omenetto, Y. Huang, Z. Kang, J. A. Rogers, *Nat. Mater.* **2010**, *9*, 929.

[5] a) T. Someya, Y. Kato, T. Sekitani, S. Iba, Y. Noguchi, Y. Murase, H. Kawaguchi, T. Sakurai, *Proc. Natl. Acad. Sci. USA* **2005**, *102*, 12321; b) T. Sekitani, H. Nakajima, H. Maeda, T. Fukushima, T. Aida, K. Hata, T. Someya, *Nat. Mater.* **2009**, *8*, 494.

[6] a) J. Hu, T. W. Odom, C. M. Lieber, *Acc. Chem. Res.* **1999**, *32*, 435; b) Y. Huang, C. M. Lieber, *Pure Appl. Chem.* **2004**, *76*, 2051.

[7] P. Staszczuk, B. Janczuk, E. Chibowski, *Mater. Chem. Phys.* **1985**, *12*, 469.

[8] S.-H. Hur, D.-Y. Khang, C. Kocabas, J. A. Rogers, *Appl. Phys. Lett.* **2004**, *85*, 5730.

[9] Z. Fan, J. C. Ho, Z. A. Jacobson, R. Yerushalmi, R. L. Alley, H. Razavi, A. Javey, *Nano Lett.* **2008**, *8*, 20.

[10] O. Wunnicke, *Appl. Phys. Lett.* **2006**, *89*, 083102.

[11] a) Z.-J. Li, Z. Qin, Z.-H. Zhou, L.-Y. Zhang, Y.-F. Zhang, *Nanoscale Res. Lett.* **2009**, *4*, 1434; b) S. Ju, P. Chen, C. Zhou, Y. Ha, A. Facchetti, T. J. Marks, S. K. Kim, S. Mohammadi, D. B. Janes, *Appl. Phys. Lett.* **2008**, *92*, 243120; c) Z. W. Chen, Z. Jiao, M. H. Wu, C. H. Shek, C. M. L. Wu, J. K. L. Lai, *Mater. Chem. Phys.* **2009**, *115*, 660.